PHYSICAL REVIEW B VOLUME 43, NUMBER 7 1 MARCH 1991

Phonon spectra and lattice specific heats of the thallium-based high-temperature superconductors

A. D. Kulkarni and F. W. de Wette
Department of Physics, University of Texas, Austin, Texas 78712-1081

J. Prade* and U. Schröder
Universität Regensburg, D-8400 Regensburg, Federal Republic of Germany

W. Kress
Max-Planck-Institut für Festkörperforschung, D-7000 Stuttgart 80, Federal Republic of Germany
(Received 20 September 1990)

We present the phonon-dispersion curves, the one-phonon densities of state, the lattice specific heat $c_v(T)$, and the Debye temperatures $\Theta(T)$ of the thallium-based high-temperature superconductors, based on full lattice dynamical calculations. Repelling effects due to hybridization of the low-lying transverse acoustic and optical modes lead to small Debye regions of the specific heat (≤ 4 K), while the occurrence of low-lying dispersionless transverse modes in the outer parts of the Brillouin zone causes large drops in the Debye temperatures $\Theta(T)$ in the range 0 to 20 K. These effects are extremely pronounced in $Tl_2Ca_2Ba_2Cu_3O_{10}$ because of the appearance of very-low-frequency modes.

I. INTRODUCTION

In a series of recent publications[1-6] we have discussed the lattice dynamics of a variety of high-temperature superconductors. The aim was to provide, in the absence of detailed experimental phonon information on which to base the dynamical models, a sufficiently general and realistic description of the lattice dynamics of these compounds to be of use for the prediction and assignments of experimental optical modes, and to give a first idea of various phonon properties, such as phonon dispersion curves, phonon densities of states, and lattice specific heat. Due to the lack of direct experimental input information about the dynamics of the high-T_c compounds, we had to base our lattice dynamical approach on what was known about the lattice dynamics of related compounds, such as perovskites and metal oxides. It will be clear that our models may have to be extended or refined, when experimental phonon dispersion data of the high-T_c compounds themselves become generally available (as they recently have for $La_{2-x}Sr_xCuO_4$ and $YBa_2Cu_3O_7$,[7] but not yet for the thallium-based compounds). Nevertheless, the calculation and description of phonon and phonon-related data at the present state of knowledge is useful, both as a possible stimulus and guide to experimentalists, and to have a "normal" lattice dynamical baseline against which to judge future experimental findings and possibly anomalous behavior.

We base our calculations on the use of interaction potentials between pairs of ions. We separate these potentials into long-range Coulomb parts and short-range overlap parts for which we assume Born-Mayer potentials. The latter are to a large extent independent of the spatial environment of the interacting ion pair and can therefore with very minor modifications be transferred from one compound to another. In addition to the two-body potentials, we take into account displacement-induced deformations of the electronic charge density in the framework of a shell model. Because of the use of short-range potentials, the eigenvalues (frequencies) and eigenvectors are obtained in the same approximation, assuring that the latter have real physical meaning. This is by no means assured for the eigenvectors obtained from force constant models for complicated structures like high-T_c compounds, even when fitted to measured phonon dispersion curves.

In two recent publications[4,6] we presented calculations of the optical modes (Raman and infrared) of the thallium-based high-T_c compounds: $Tl_2Ba_2CuO_6$ (2:0:2:1:6), $Tl_2CaBa_2Cu_2O_8$ (2:1:2:2:8), $Tl_2Ca_2Ba_2Cu_3O_{10}$ (2:2:2:3:10) [body-centered-tetragonal (bct) structures], and $TlCaBa_2Cu_2O_7$ (1:1:2:2:7), $TlCa_2Ba_2Cu_3O_9$ (1:2:2:3:9), $TlCa_3Ba_2Cu_4O_{11}$ (1:3:2:4:11) [simple-tetragonal (st) structures]. We required that the shell models for the different high-T_c compounds which we have treated earlier [$YBa_2Cu_3O_7$ (Ref. 2) and $Bi_2CaSr_2Cu_2O_8$ (Ref. 3)] are compatible with the present calculations; this requires that the short-range potentials for given ion pairs in equivalent environments are transferable between compounds. These models reproduce the available experimental infrared and Raman data of all these compounds quite well.

In the present work we have extended the lattice dynamical calculations for the thallium-based superconductors to wave vectors over the entire Brillouin zone. This allowed us to evaluate the one-phonon density of states function for all these compounds, with the help of which the mean-squared amplitudes of vibration (entering Debye-Waller factors), and the lattice thermodynamic functions, such as the lattice specific heat, can be calculated.

In Sec. II we present the phonon dispersion curves and the one-phonon densities of states. In Sec. III we present the lattice specific heat $c_v(T)$, which is also expressed in the Debye temperature $\Theta(T)$. A discussion of these results will be given in Sec. IV.

II. LATTICE DYNAMICAL PROPERTIES

The phonon dispersion curves and densities of states are obtained from lattice dynamical calculations for an appropriate sampling grid of wave vectors in the irreducible part of the Brillouin zone (BZ). It is our experience that a model that leads to stable dynamics at the zone center (Γ) and in the symmetry directions of the BZ, often gives rise to one or more regions (pockets) of instability in the off-symmetry directions. Hence an examination of the phonon frequencies in the entire BZ is important to make sure that the lattice dynamical model is dynamically stable, i.e., that it does not give rise to any imaginary frequencies anywhere in the BZ. We emphasize that this is by no means a trivial requirement for the high-T_c superconductors, all of which appear to be, to varying degree, close to structural instability.

A. Phonon dispersion curves

In Fig. 1 we show the BZ's for the bct and st structures with the directions along which the phonon dispersion curves are displayed. In Figs. 2–4 we display the dispersion curves for the bct compounds 2:0:2:1:6, 2:1:2:2:8, and 2:2:2:3:10, and in Figs. 5–7 those for the st compounds 1:1:2:2:7, 1:2:2:3:9, and 1:3:2:4:11.

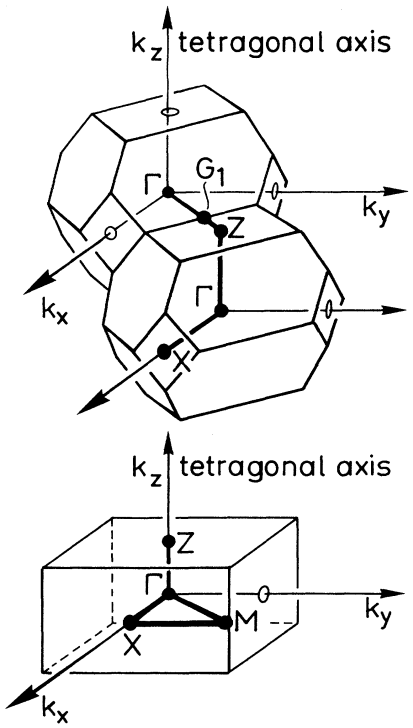

FIG. 1. Brillouin zones of the body-centered tetragonal (top) and simple tetragonal (bottom) lattices. The symmetry directions along which the dispersion curves are displayed are indicated with heavy lines. For the body-centered tetragonal lattice, $X=(1,1,0)\pi/a$, $G_1=(1,0,0)(1+a^2/c^2)\pi/a$, and $Z=(0,0,2)\pi/c=(2,0,0)\pi/a$. For the simple tetragonal lattice, $X=(1,0,0)\pi/a$, $M=(1,1,0)\pi/a$, and $Z=(0,0,1)\pi/c$. a,a,c are the sides of the *conventional* unit cells of both lattices.

These figures are shown to exhibit the overall features of the dispersion curves. In the computer-generated plots the frequencies at neighboring wave-vector points were connected according to successive magnitude rather than to their representation. In a few isolated instances this may not lead to the correct crossing behavior but in most of these cases it is quite evident which curves should be connected (in such a fashion).

The hybridization of the low-lying acoustic and optical modes in the neighborhood of Γ is of special interest, since it has a direct bearing on the low-temperature specific heat. This behavior is particularly pronounced for the bct compounds in the ΓG_1 and ΓX directions of the Brillouin zone. Going through the series 2:0:2:1:6, 2:1:2:2:8, to 2:2:2:3:10 we see that the lowest transverse acoustic mode near Γ is increasingly pushed down by hybridization with the low-lying transverse optical mode of the same representation (lying above 2 THz). This repelling of modes causes an onset of curvature in the dispersion curves already below 0.4 THz. This curvature is the cause of the unusually small Debye region (0–4 K) of the lattice specific heat of these compounds. We note that for the st compounds the hybridization behavior near Γ does not change much as we go through the series

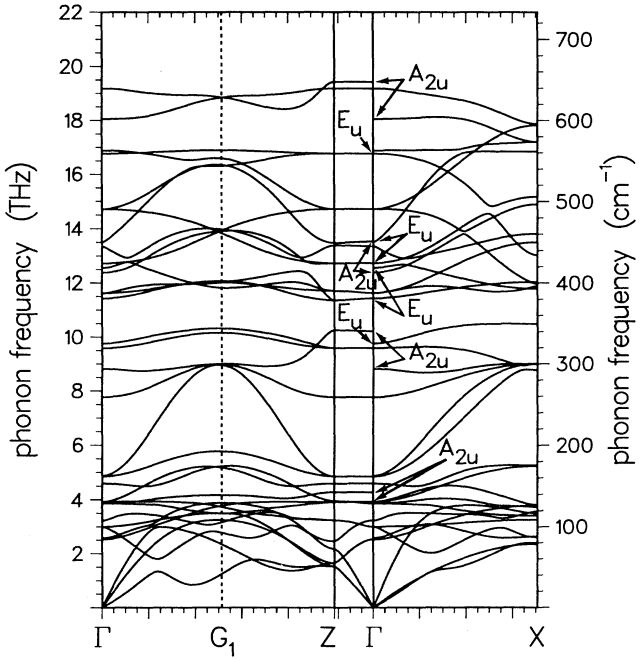

FIG. 2. Phonon dispersion curves of bct $Tl_2Ba_2CuO_6$ (2:0:2:1:6) along symmetry directions of the bct BZ (cf. Fig. 1). Successive tick marks along the horizontal axis are separated by $0.1\pi/a$. At Γ the LO-TO splitting of some of the infrared-active modes is indicated. (In all cases the LO is the upper and the TO is the lower frequency.)

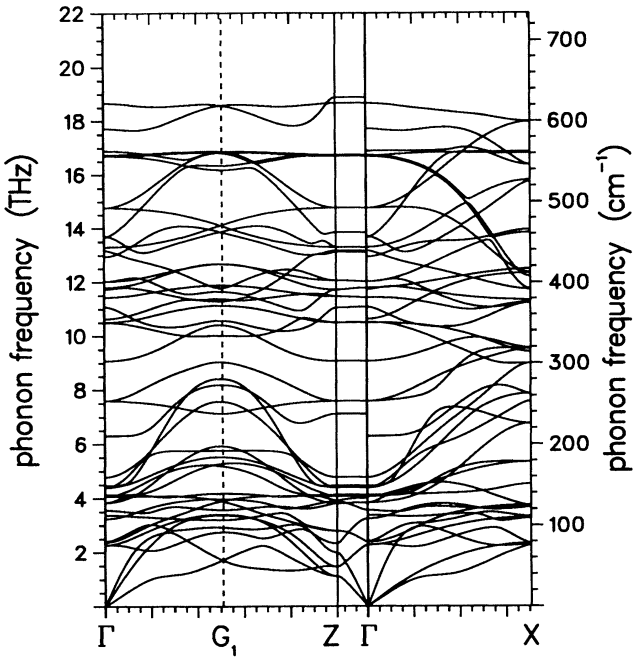

FIG. 3. Phonon dispersion curves of bct $Tl_2CaBa_2Cu_2O_8$ (2:1:2:2:8) along symmetry directions of the bct BZ.

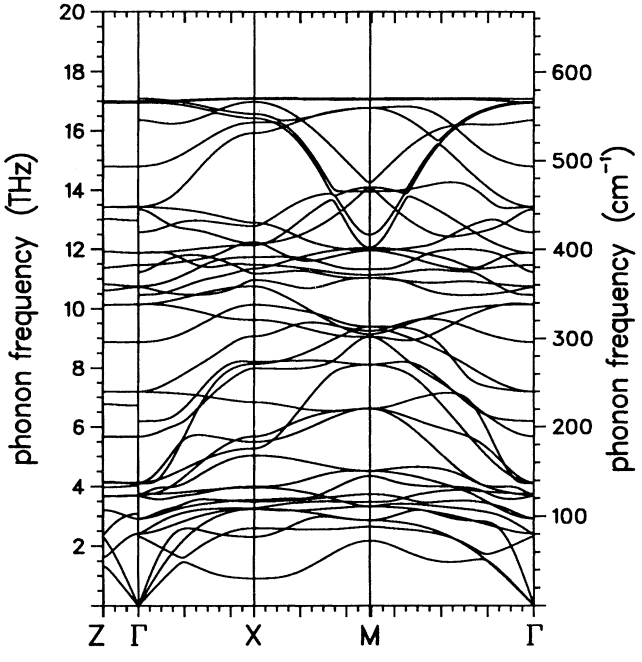

FIG. 5. Phonon dispersion curves of st $TlCaBa_2Cu_2O_7$ (1:1:2:2:7) along symmetry directions of the st BZ.

1:1:2:2:7, 1:2:2:3:9, to 1:3:2:4:11. The bct and st structures have in common that in the outer parts of the zone, the lowest modes are these hybridized optical modes, which only show weak dispersion. The contributions of these flat parts of the dispersion curves to the specific heat give rise to the steep drop in the Debye temperature $\Theta(T)$ in the temperature range 3 to 20 K.

Another phenomenon which is quite evident from the dispersion curves is the LO-TO splitting of the optical modes, which shows up in Figs. 2, 3, and 4 as discontinuities at Γ in some of the dispersion curves along the ΓZ and ΓX directions. Since Fig. 2 is the simplest, we have

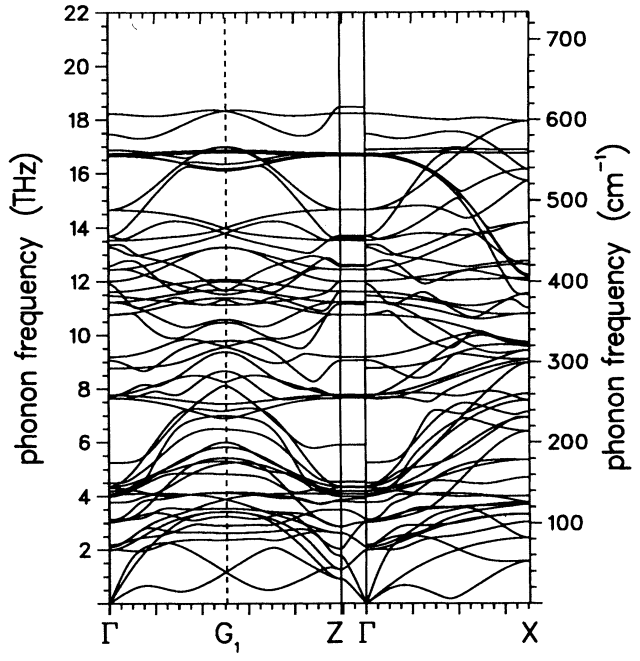

FIG. 4. Phonon dispersion curves of bct $Tl_2Ca_2Ba_2Cu_3O_{10}$ (2:2:2:3:10) along symmetry directions of the bct BZ.

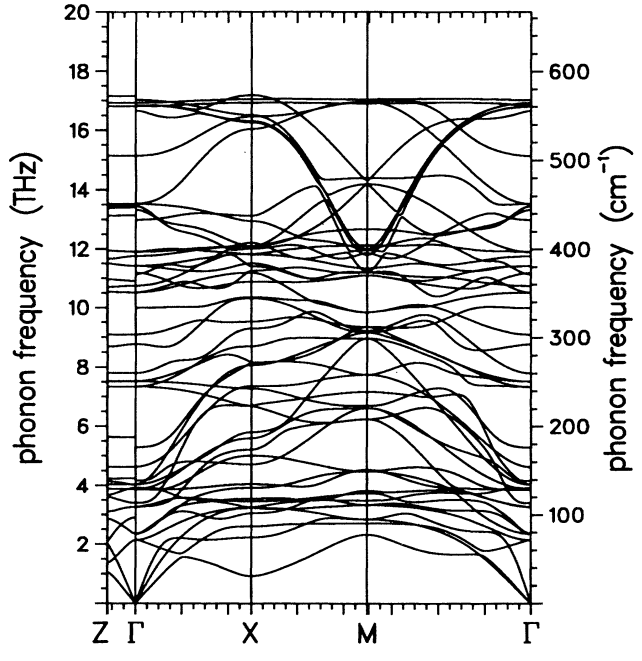

FIG. 6. Phonon dispersion curves of st $TlCa_2Ba_2Cu_3O_9$ (1:2:2:3:9) along symmetry directions of the st BZ.

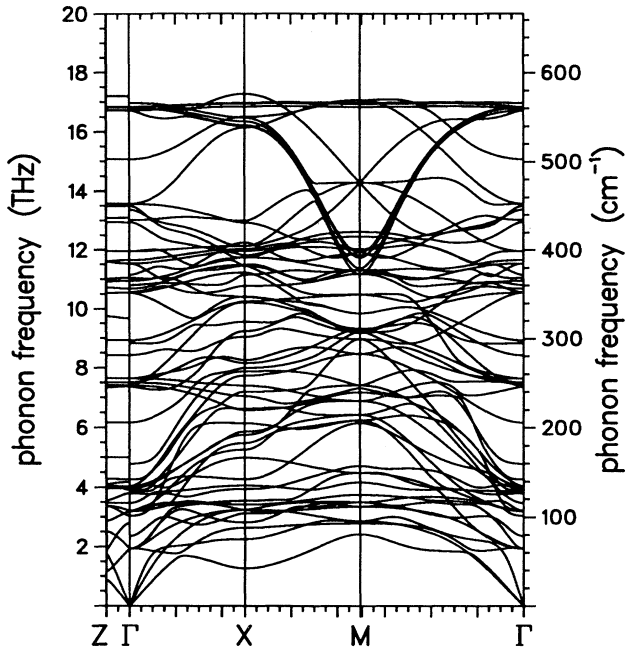

FIG. 7. Phonon dispersion curves of st $TlCa_3Ba_2Cu_4O_{11}$ (1:3:2:4:11) along symmetry directions of the st BZ.

indicated some of these LO-TO splittings. Their assignments can be conveniently checked in Tables IV and V of Ref. 6, which refer to the infrared-active optical modes. We point out that the dispersion diagram of Fig. 2 is the only one showing an absolute gap (between 350 cm^{-1} and 380 cm^{-1}). It is seen in the density of states curve for 2:0:2:1:6 (Fig. 8) that this gap extends through the entire Brillouin zone. Figures 3 and 4 are in most aspects similar to Fig. 2 but show increasing complication, due to the increasing number of particles in the unit cell. However Fig. 4 for 2:2:2:3:10 shows an unusual feature, namely, a fairly soft mode between Γ and the zone boundary (G_1 and X) which is particularly pronounced along ΓX. We will see below that this soft mode causes an anomalous behavior of the lattice specific heat of 2:2:2:3:10. It is interesting to note that Koyama and Hoshiya[8] have seen evidence of such a soft mode in thermal diffuse electron scattering of 2:2:2:3:10. Inelastic neutron scattering measurements of the phonon dispersion curves will be needed, in addition, to unambiguously establish the existence and the precise location in the BZ of such a soft mode.

The dispersion curves for the st structures 1:1:2:2:7, 1:2:2:3:9, and 1:3:2:4:11 (see Figs. 5–7) are quite similar to each other, expect for the increasing complexity due to the increasing number of particles in the unit cell.

We point out that the dispersion curves displayed here were obtained with a straightforward lattice dynamical calculation which only includes electron-phonon interactions of dipolar symmetry. As experimental phonon dispersion curves become available, interactions of other than dipolar symmetry may turn out to be important, as recent inelastic neutron scattering studies[7] of $La_{2-x}Sr_xCuO_4$ and $YBa_2Cu_3O_{7-\delta}$ seem to indicate. In such cases our model can be extended in a natural way to include electron-phonon couplings of monopolar and quadrupolar symmetry.

B. Phonon densities of states

The one-phonon densities of states (PDOS) of all six thallium-based compounds are displayed in Fig. 8, with those for the bct structures on the left and those for the st structures on the right. There are a few striking similarities between these diagrams. For instance, the sharp peak around 560 cm^{-1} appearing in all diagrams is the O(1) stretch vibration[9] which is practically dispersionless (cf. Figs. 2–7), and which is the infrared-active E_u mode at Γ (cf. Ref. 6, Table V). In the bct compounds there is a small structure at and above 600 cm^{-1} which is mainly due to the O(3) z vibration,[9] which is the Raman-active A_{1g} mode or the infrared-active A_{2u} mode at Γ (cf. Ref. 6, Tables II and IV). In the st compounds, the frequency of these O(3) vibrations are lower and they contribute to the broad peak just on the left of the sharp peak at 560 cm^{-1} in the st diagrams. Another point of interest, already mentioned above, is the presence of an absolute gap in the PDOS of 2:0:2:1:6. The peak just below the gap at about 350 cm^{-1} is an O(1) angle-bend mode, which is the infrared-active 320–326 cm^{-1} E_u mode at Γ.

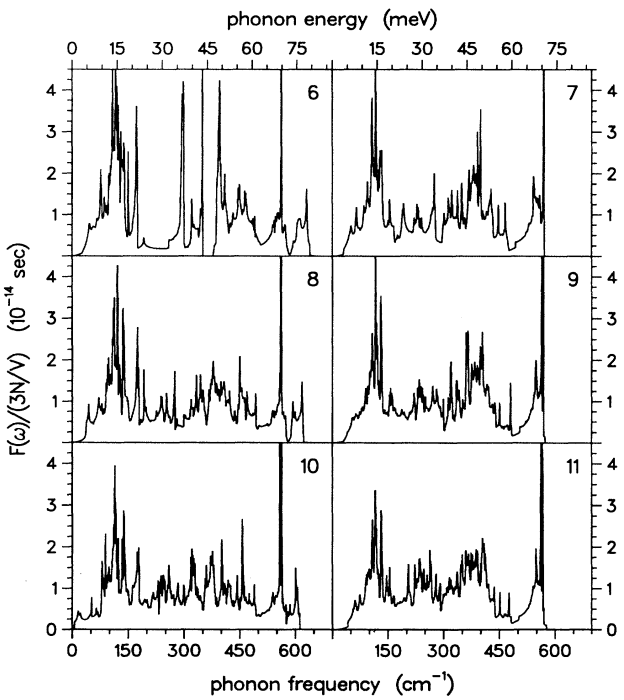

FIG. 8. Normalized one-phonon densities of states [in units $1/(10^{14}$ rad/sec)] of the thallium-based superconductors. The normalization factor $3N/V$ makes the area under each curve unity (N is the number of particles in the unit cell and V its volume). The numbers 6,7, $\cdots$ identify the compounds according to oxygen formula number. Left-hand panels: bct structures; right hand panels: st structures.

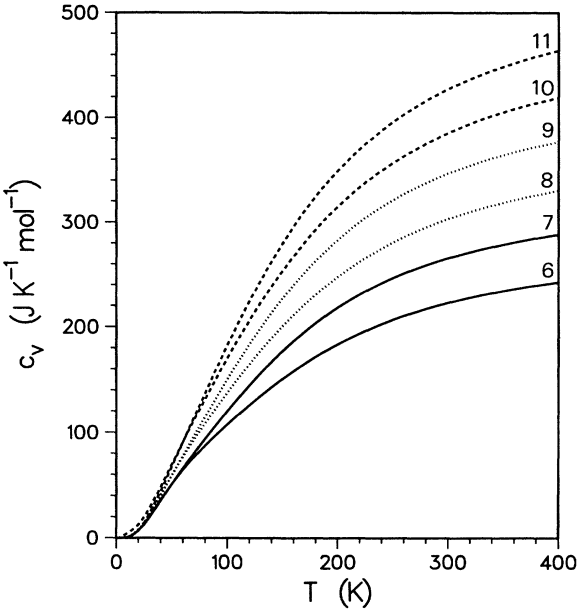

FIG. 9. Specific heat functions $c_v(T)$ of the thallium-based superconductors in J K^{-1} mol^{-1} in the temperature range 0–400 K. The numbers 6,7,... identfy the compounds according to the oxygen formula number.

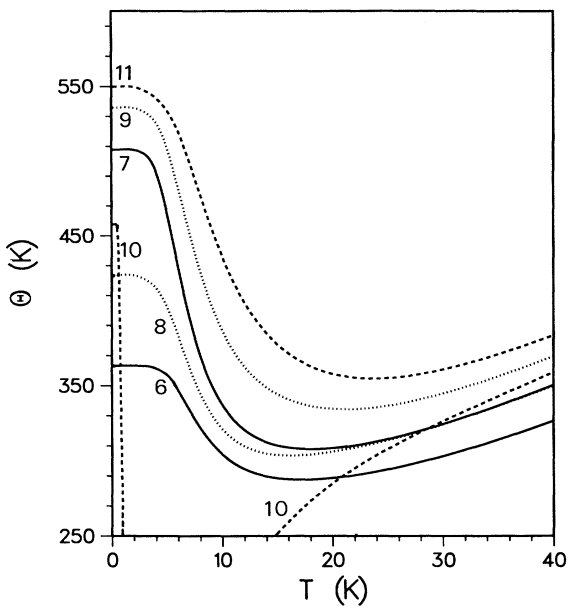

FIG. 11. $\Theta(T)$ in the temperature range 0–40 K.

We note in passing, that the existence of an absolute gap can facilitate the appearance of vibrational modes that are strongly localized at the surface.

It can be seen from the phonon dispersion curves that many of the optical modes have very little dispersion, and this gives rise to sharp peaks in the PDOS.

Finally we draw attention to the low-frequency structure in the PDOS of 2:2:2:3:10. This structure is caused by the very low-lying modes which were already commented on in the discussion of Fig. 4. In Sec. III we will see that these modes give rise to an anomalously large lattice specific heat of 2:2:2:3:10 [i.e., low $\Theta(T)$] at low temperatures.

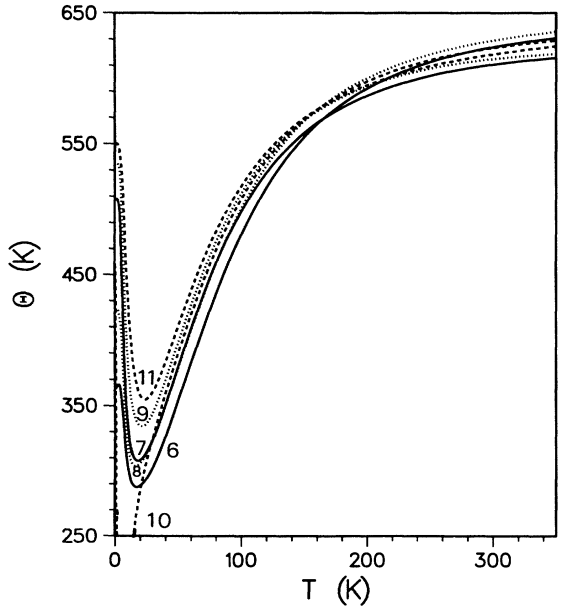

FIG. 10. Temperature-dependent Debye temperature $\Theta(T)$ of the thallium-based superconductors, in K, in the temperature range 0–350 K. Identification of the curves is as in Fig. 9.

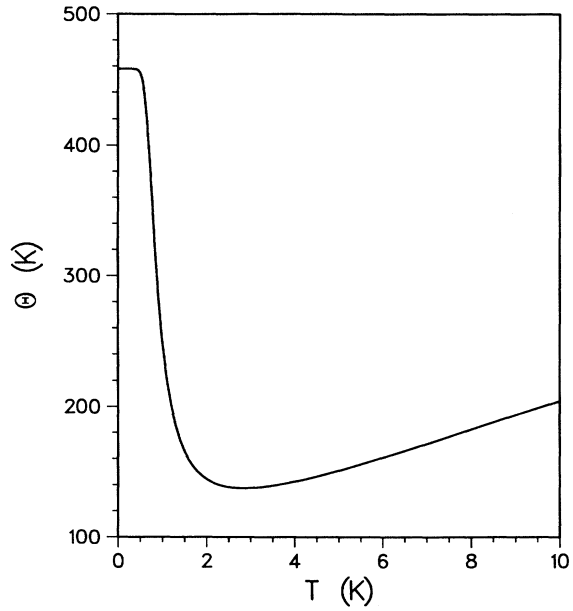

FIG. 12. $\Theta(T)$ of $Tl_2Ca_2Ba_2Cu_3O_{10}$ (2:2:2:3:10) in the temperature range 0–10 K.

TABLE I. Debye temperature $\Theta(0)$, extent T_{max} of the Debye region (defined by the condition $\Theta(T)\approx\Theta(0)$ for $T\leq T_{max}$), minimum Debye temperature Θ_{min}, temperature T_{min} at which Θ_{min} occurs, and *relative drop* $[\Theta(0)-\Theta_{min}]/\Theta(0)$. All temperatures are expressed in K.

			Extent of Debye region				
	Compound	$\Theta(0)$	T_{max}	$T_{max}/\Theta(0)$	Θ_{min}	T_{min}	Relative drop
bct	2:0:2:1:6	363	4.0	0.011	287	17.0	21%
	2:1:2:2:8	424	2.4	0.006	303	16.0	29%
	2:2:2:3:10	458	0.45	0.001	137	2.8	70%
st	1:1:2:2:7	508	2.4	0.005	308	18.0	39%
	1:2:2:3:9	536	2.4	0.004	334	21.0	38%
	1:3:2:4:11	550	2.4	0.004	355	24.0	35%

III. LATTICE SPECIFIC HEATS

The lattice specific heat $c_v(T)$ is evaluated by substituting the PDOS $F(\omega)$ in the familiar expression

$$c_v(T)=\frac{k_B^2 T}{\hbar}\int_0^\infty \frac{x^2 e^x}{(e^x-1)^2} F\left[x\frac{k_B T}{\hbar}\right]dx \ , \qquad (1)$$

where $x=\hbar\omega/k_B T$. Unfortunately, for very low temperatures the practical use of Eq. (1) leads to numerically inacccurate results, because of inaccuracies in the calculated $F(\omega)$ for very small ω. These inaccuracies result from the fact that the root sampling method [used to evaluate $F(\omega)$] terminates $F(\omega)$ at some lowest frequency ω_{min}. For temperatures smaller than $\hbar\omega_{min}/k_B$, c_v as given by Eq. (1) will become anomalously small. Therefore, we have chosen sampling meshes in the BZ in such a way that ω_{min} lies in the linear dispersion region of the acoustic modes. In this region the Debye approximation is strictly valid, and we have used the method of de Wette *et al.*[10] to give low-temperature results for $c_v(T)$ to any desired accuracy.

As it turns out, plots of the $c_v(T)$ functions for the various thallium-based compounds (Fig. 9) all look quite similar and are therefore not very instructive. In contrast, both c_v/T^3 and the Debye temperature $\Theta(T)$ are much more revealing, in that they display in one glance the extent of the Debye region [where $\Theta(T)\approx\Theta(0)$, the "initial" Debye temperature] and the deviations from Debye behavior. $\Theta(T)$ is obtained by equating at each temperature, the Debye specific-heat expression

$$c_v^D(T)=9k_B\frac{N}{V}\left[\frac{T}{\Theta}\right]^3\int_0^{\Theta/T}\frac{x^4 e^x}{(e^x-1)^2}dx \qquad (2)$$

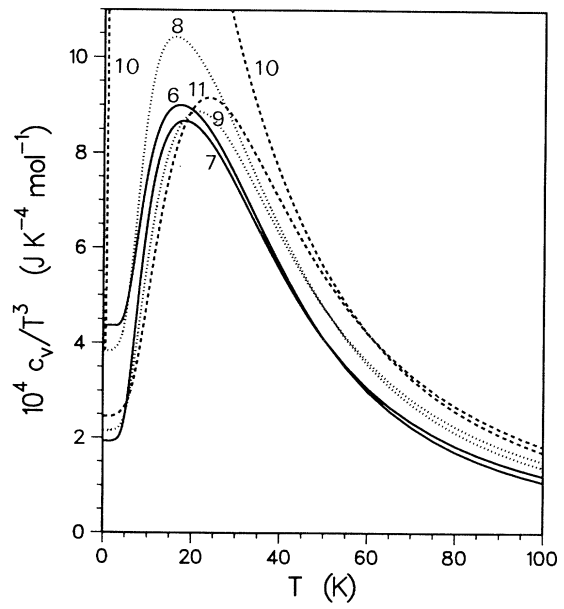

FIG. 13. c_v/T^3 in 10^{-4} J K^{-4} mol^{-1} vs T in the temperature range 0–100 K.

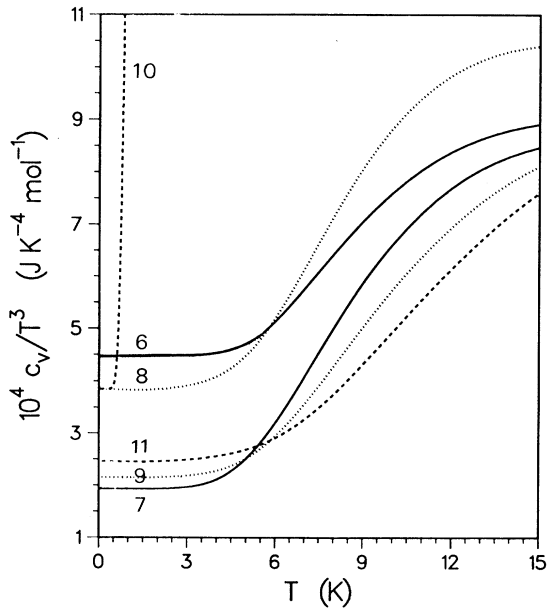

FIG. 14. c_v/T^3 in 10^{-4} J K^{-4} mol^{-1} vs T in the temperature range 0–15 K.

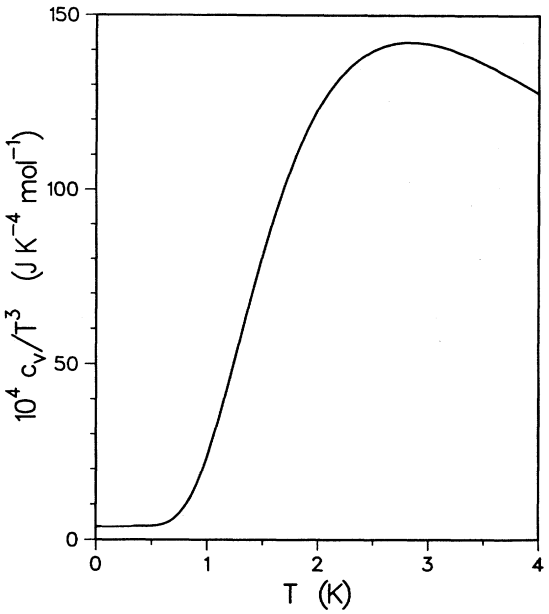

FIG. 15. c_v/T^3 in 10^{-4} J K^{-4} mol^{-1} vs T for $Tl_2Ca_2Ba_2Cu_3O_{10}$ (2:2:2:3:10) in the temperature range 0–4 K.

to the calculated value of $c_v(T)$, and inverting Eq. (2) to obtain $\Theta(T)$ (N is the number of particles in the unit cell and V its volume).

In Fig. 10 we show the $\Theta(T)$ curves for five thallium-based compounds in the temperature range 0–350 K. In Fig. 11 these same functions are given in the range 0–40 K, and in Fig. 12 for 2:2:2:3:10 in the range 0–10 K. The extent of the Debye region ($T_{\max}$), Debye temperature $\Theta(0)$, and minimum Debye temperature $\Theta_{\min}(T_{\min})$ are given in Table I.

Overall these results display the same characteristics as we found recently for the specific heat of $YBa_2Cu_3O_7$.[11]

(1) The Debye regions are quite small, ranging from 0.011 $\Theta(0)$ for 2:0:2:1:6 to the anomalously low value of 0.001 $\Theta(0)$ for 2:2:2:3:10.

(2) The drop in $\Theta(T)$ at low temperatures in percentage of $\Theta(0)$ is large, ranging from 21% for 2:0:2:1:6 to the anomalously large value of 70% for 2:2:2:3:10. The small extent of these Debye regions is a result of the onset of curvature in the acoustic dispersion curves at quite low frequencies, while the extent of the drop in $\Theta(T)$ at low temperatures is the result of the low lying modes in large parts of the BZ.

In Fig. 13 we display the functions $c_v(T)/T^3$ versus T. They are of interest, not only because they show very clearly the extent of the Debye region $c_v \approx \beta T^3$, but also because they give an indication about the T-power behavior of c_v just outside the Debye region. This is particularly clear in Fig. 14 where c_v/T^3 versus T is shown in the range 0–15 K. Because of its very small Debye region, the c_v/T^3 curve for 2:2:2:3:10 in the range 0–4 K is shown in Fig. 15.

As we recently found for $YBa_2Cu_3O_7$,[11] the functions c_v/T^3 show a region of linear behavior just above the Debye region, which means that in that region c_v would be quite well represented by the function $\beta' T^3 + \delta T^4$ [β' is different from β in βT^3, which gives the best fit in the Debye region and thus is associated with the Debye temperature $\Theta(0)$]. This unusual behavior of the lattice specific heat at low temperatures, namely, very small Debye region, T^4 behavior just outside this region, and a more complicated T behavior at somewhat higher (but still low) temperatures, should make it clear that fitting of the measured low-temperature specific heats, which contain these complicated lattice contributions, requires much care, both with regard to fitting functions and fitting regions. Fitting with the wrong function or in the wrong temperature range can easily lead to erroneous conclusions about the existence of anomalous contributions to the specific heat.

IV. DISCUSSION

In this paper we have presented results for phonon and phonon-related properties of the thallium-based high-T_c superconductors. These results were obtained with lattice dynamical calculations based on shell models, employing ionic interaction potentials which are common to a broad class of high-T_c superconductors. We obtained an overall consistent description of the lattice dynamics of these compounds, leading to reasonable agreement with the experimental data on optical phonons and the specific heat. Undoubtedly, when measured phonon dispersion curves become available, our models for individual compounds may have to be refined or extended, for instance, to account for the presence of electron-phonon anomalies. There are, in fact, a variety of ways in which electron-phonon anomalies can be accounted for in the framework of the shell model, such as the introduction of higher (than dipole) deformabilities of the ionic charge distributions. Of course, partial (two-dimensional) screening can also be incorporated in the calculations, if needed.

We expect, however, that any of the model refinements alluded to above will affect the phonon dispersion behavior only in rather restricted parts of wave-vector space. As a consequence, they will have only small effects on the densities of states and the specific heat. The important conclusions of this paper regarding the specific heat, namely, the existence of an anomalously small Debye region and anomalously varying Debye temperatures just above this region, will remain unchanged. They are due, respectively, to hybridization of acoustic and optical modes near the center of the Brillouin zone, and to the appearance of low-lying transverse modes with low dispersion. These are general dynamical characteristics of these complicated structures which will not be changed by small changes in the phonon spectra.

ACKNOWLEDGMENTS

This work was partially supported by the National Science Foundation through Grant No. DMR-8816301, by the Robert A. Welch foundation through Grant No. F-433, by the Deutsche Bundesministerium für Forschung und Technologie, and by a NATO Travel Grant. Acknowledgment is also made to the donors of the Petroleum Research Fund, administered by the American Chemical Society, for partial support of this research.

*Present address: Siemens AG, Munich, Federal Republic of Germany.

[1]J. Prade, A. D. Kulkarni, F. W. de Wette, W. Kress, M. Cardona, R. Reiger, and U. Schröder, Solid State Commun. **64**, 1267 (1987).

[2]W. Kress, U. Schröder, J. Prade, A. D. Kulkarni, and F. W. de Wette, Phys. Rev. B **38**, 2906 (1988).

[3]J. Prade, A. D. Kulkarni, F. W. de Wette, U. Schröder, and W. Kress, Phys. Rev. B **39**, 2771 (1989).

[4]A. D. Kulkarni, J. Prade, F. W. de Wette, W. Kress, and U. Schröder, Phys. Rev. B **40**, 2642 (1989).

[5]W. Kress, J. Prade, U. Schröder, A. D. Kulkarni, and F. W. de Wette, Physica C **162 - 164**, 1345 (1989).

[6]A. D. Kulkarni, F. W. de Wette, J. Prade, U. Schröder, and W. Kress, Phys. Rev. B **41**, 6409 (1990).

[7]L. Pintschovius, in *Proceedings of the Third International Conference on Phonon Physics (Phonons 89)*, edited by S. Hunklinger, W. Ludwig, and G. Weiss (World Scientific, Singapore, 1990), p. 217.

[8]Y. Koyama and H. Hoshiya, Phys. Rev. B **39**, 7336 (1989).

[9]O(1) are the oxygen atoms in those Cu-O planes that are adjacent to the Ba-O planes. O(3) are the oxygen atoms in the Tl-O planes. For more information, cf. Ref. 6, Fig. 1.

[10]F. W. de Wette, L. H. Nosanow, and N. R. Werthamer, Phys. Rev. **162**, 824 (1967).

[11]F. W. de Wette, A. D. Kulkarni, J. Prade, U. Schröder, and W. Kress, Phys. Rev. B **42**, 6707 (1990).